Spin dynamics of the frustrated integer spin antiferromagnetic Heisenberg chain

2007 J. Phys.: Condens. Matter 19 276207

(http://iopscience.iop.org/0953-8984/19/27/276207)

IOP PUBLISHING JOURNAL OF PHYSICS: CONDENSED MATTER

J. Phys.: Condens. Matter **19** (2007) 276207 (16pp) doi:10.1088/0953-8984/19/27/276207

Spin dynamics of the frustrated integer spin antiferromagnetic Heisenberg chain

G M Rocha-Filho[1], M E Gouvêa[2] and A S T Pires[1]

[1] Departamento de Física, ICEx, Universidade Federal de Minas Gerais, Avenida Antônio Carlos 6627, CEP:31270-901, Belo Horizonte, MG, Brazil
[2] Centro Federal de Educação Tecnológica de Minas Gerais, Av. Amazonas 7675, CEP:30510-000, Belo Horizonte, MG, Brazil

E-mail: gmrocha@fisica.ufmg.br, meg@dppg.cefetmg.br and antpires@fisica.ufmg.br

Received 22 February 2007, in final form 4 May 2007
Published 21 June 2007
Online at stacks.iop.org/JPhysCM/19/276207

Abstract

We present low-temperature static and dynamic properties of the quantum one-dimensional isotropic integer spin Heisenberg magnet with antiferromagnetic nearest-neighbour (nn) and next-nearest-neighbour (nnn) interactions. The modified spin-wave theory is used to provide quantities such as the spin-wave dispersion relation, the ground-state energy, the gap and its dependence with temperature, and the asymptotic behaviour of the spin–spin correlation function. The ground state energy and the singlet–triplet energy gap are obtained for several values of j, defined as the ratio of the nnn interaction constant to the nn one. Our results show that the ground-state and the gap energies increase with j, in accordance with numerical results available in the literature. The calculation of the dynamic correlation function is performed using the projection operator formalism: the procedure includes up to two-magnon processes. We show that, depending on the values of the frustration parameter j, the wavevector and the temperature, a double-peak structure for the dynamical correlation function can develop.

1. Introduction

The physics of low-dimensional quantum magnets has revealed many interesting and unexpected behaviours, stimulating a great number of theoretical, numerical and experimental studies in the area. Among the systems that have deserved attention for their rich behaviour are those that, due to the symmetry of the lattice or to competing interactions between the spins of the system, present some degree of frustration. Concerning antiferromagnetic systems, our interest in this work, frustration tends to suppress antiferromagnetic correlations, and, therefore, the tendency towards the Néel order. Then, as frustration is increased, the ground state of the system can change and a quantum phase transition may occur. In quantum systems, the interplay of frustration and quantum fluctuations may lead to a spin-liquid state or to some kind of spontaneous symmetry breaking.

One of the simplest quantum frustrated systems that has deserved great attention is the quantum isotropic Heisenberg spin chain with antiferromagnetic nearest-neighbour (nn) and next-nearest-neighbour (nnn) interactions. In the absence of frustration, the antiferromagnetic Heisenberg chain is known to have quite different properties for integer or half-integer spins: the so-called Haldane's conjecture [1]. Then, it is natural to expect different behaviours for frustrated Heisenberg chains involving integer or half-integer spins, and the knowledge achieved in the field corroborates this expectation. The ground state of half-integer spin frustrated chains is either in the spin-fluid phase [2] or in the dimer phase [3, 4], depending on whether j, the ratio of the nnn interaction constant to the nn one, is smaller or larger than a critical value $j_c \approx 0.241$ [5, 6].

The ground-state properties of the spin-1 frustrated chain were first investigated by Tonegawa *et al* [7], and the phase diagram was finally clarified by Kolezhuk *et al* [8]. Analytical methods [9, 10] predicted a gap for any value of frustration, and this fact was confirmed by numerical studies [7, 8]. The phase diagram of the integer spin antiferromagnetic Heisenberg one-dimensional model has three special points [8]. At $j_D = 0.284(1)$, there is a disorder point of the first kind, signalling the onset of incommensurate spin–spin correlations in the chain. A Lifshitz point at $j_L = 0.3725(25)$ is identified by the appearance of a doubly degenerate structure in the excitation spectrum leading to the emergence of a two-peak structure in the $S(q)$ structure function. The third special point at $j_T = 0.7444(6)$ is related to a phase transition from the Haldane (or Affleck–Kennedy–Lieb–Tasaki [11]—AKLT) phase to the next-nearest-neighbour AKLT phase. The Haldane phase, $j < j_T$, is characterized by a finite value of the string order parameter [12]; at j_T this order parameter goes to zero, and the phase transition was initially identified [8] as a first-order transition. Later, Kolezhuk and Shollwöck [13] showed that the order parameter of the large-j phase is related to two intertwined strings and that the phase transition has a topological nature. A rich phase diagram was also found for the frustrated XXZ antiferromagnetic spin $S = 1$ chain by using the density matrix renormalization group method [14]. The ground state of this model shows six different phases: the Haldane, gapped chiral, gapless chiral, double Haldane, Néel, and double Néel.

However, despite the enormous progress achieved in the understanding of the ground-state properties of the spin-1 frustrated antiferromagnetic Heisenberg one-dimensional model, results describing the dynamics of such a model are still missing—even in an approximate framework. In the present work, we calculate the dynamical correlation function of this model using the equation of motion approach in conjunction with projection operator methods, following a procedure proposed originally by Reiter [15] and further developed by other authors [16]. This method is not limited to short-time and short-distance behaviour and has proven successful in the study of the classical and quantum Heisenberg models in one [17] and two dimensions [18, 19], showing good agreement with experimental data, molecular dynamic simulations, and, also, with other theories [20].

The calculation of the memory function, which plays a central role in the formalism, does not require long-range order to be valid because it depends only on correlations between first and second neighbours. The frequency of the local spin-wave modes and static correlations are required as input to the method and, in this work, are obtained via the modified spin-wave (MSW) treatment instead of using the standard spin-wave theory, as usual. It is well known that the standard spin-wave theory is not applicable to low-dimensional quantum magnets without modifications [21]. In the MSW theory [22], the consequence of the Mermin–Wagner theorem is enforced by hand in a variational density matrix approach. The procedure has been applied to one- (1D) and two-dimensional (2D) ferro- [22] and antiferromagnets [23, 24], giving results in excellent agreement with results obtained via exact diagonalization [25] and renormalization group theory [26]. The phase diagram of the 2D frustrated Heisenberg spin $S = 1/2$ model

was obtained [27] by means of the MSW approach. Some of us [28] applied the method to the non-frustrated 1D, spin-1, Heisenberg model to obtain the dependence of the gap as a function of the temperature and the comparison to experimental data [29] obtained for the Y_2BaNiO_5 compound is acceptable. Besides using the MSW theory to obtain the quantities required by the memory function formalism, we also use it to calculate other quantities related to the ground state of the model, showing that this simple theory gives good estimates for the ground-state energy and for the asymptotic behaviour of the spin–spin correlation function. The dependence of the gap with temperature and with the frustration parameter is in qualitative agreement with other numerical data [7, 30].

The combination of these two techniques, the projection operator method and the MSW theory, was already applied by some of us to study the low-temperature properties of the quantum 1D spin-1 [28] and 2D (finite-T) spin-1/2 [19] Heisenberg models, where a gap is expected to occur. The projection operator method takes into account, properly, the effects due to magnon scattering in the calculation of the dynamical structure function, as will be discussed, in more detail, in section 3. The procedure adopted in this paper is valid for integer spins. However, in our calculations, we have used $S = 1$.

The paper is organized as follows. In section 2, we briefly review the MSW theory and discuss the results obtained for the ground-state energy, the gap, and the spin–spin correlation function for several values of the frustration parameter, j. The projection operator method and the results obtained for the dynamical correlation function are discussed in section 3. Our conclusions are presented in section 4.

2. Modified spin-wave theory and results

The Hamiltonian describing the antiferromagnetic frustrated Heisenberg chain can be written as

$$H = J_1 \sum_l \{[\mathbf{T}_{2l} \cdot \mathbf{S}_{2l+1} + \mathbf{S}_{2l+1} \cdot \mathbf{T}_{2l+2}] + j[\mathbf{T}_{2l} \cdot \mathbf{T}_{2l+2} + \mathbf{S}_{2l+1} \cdot \mathbf{S}_{2l+3}]\}, \tag{1}$$

where the sum runs over all l sites of each sublattice, $\mathbf{T}_{2l}$ and $\mathbf{S}_{2l+1}$ denote the spins in the two different sublattices, and j is the frustration parameter defined as $j = J_2/J_1$, where J_1 and J_2 are, respectively, the antiferromagnetic nn and nnn coupling constants.

We now apply the Dyson–Maleev transformation to represent the spin operators in each antiferromagnetic sublattice in terms of bosonic operators, writing

$$\begin{aligned} T^-_{2l} &= a^\dagger_{2l}; \qquad & T^\dagger_{2l} &= (2S - a^\dagger_{2l} a_{2l}) a_{2l}, \\ T^z_{2l} &= S - a^\dagger_{2l} a_{2l}; \qquad & S^z_{2l+1} &= -S + b^\dagger_{2l+1} b_{2l+1}; \\ S^-_{2l+1} &= -b_{2l+1}; \qquad & S^\dagger_{2l+1} &= -b^\dagger_{2l+1}(2S - b^\dagger_{2l+1} b_{2l+1}). \end{aligned} \tag{2}$$

Using (2), Hamiltonian (1) has no term higher than the fourth order, and we construct a self-consistent theory instead of a conventional $1/S$ expansion. In terms of these bosonic operators, the Hamiltonian has now the form

$$H = E_0 + H_0 + H_1, \tag{3}$$

where $E_0 = -2J_1 N S^2 (1 - j)$, N is the number of spins in each sublattice, and H_0 and H_1 represent terms of the Hamiltonian involving, respectively, products of two and four bosonic operators. The expressions for these two terms are

$$\begin{aligned} H_0 = J_1 S \sum_l \{&2b^\dagger_{2l+1} b_{2l+1} + 2a^\dagger_{2l} a_{2l} - (a_{2l} + a_{2l+2}) b_{2l+1} - (a^\dagger_{2l} + a^\dagger_{2l+2}) b^\dagger_{2l+1} \\ &- j[(a^\dagger_{2l+2} - a^\dagger_{2l})(a_{2l+2} - a_{2l}) + (b^\dagger_{2l+1} - b^\dagger_{2l+3})(b_{2l+1} - b_{2l+3})]\} \end{aligned} \tag{4}$$

and

$$H_1 = \frac{J_1}{2}\sum_l \{a_{2l}^\dagger (b_{2l+1}^\dagger - a_{2l})^2 b_{2l+1} + a_{2l+2}^\dagger (b_{2l+1}^\dagger - a_{2l+2})^2 b_{2l+1} - j[a_{2l}^\dagger a_{2l+2}^\dagger (a_{2l} - a_{2l+2})^2 + (b_{2l+1}^\dagger - b_{2l+3}^\dagger)^2 b_{2l+1} b_{2l+3}]\}. \tag{5}$$

Following Takahashi [24], we now introduce an ideal spin-wave ansatz for the density matrix of the system,

$$\rho = \exp\left(\frac{1}{T}\sum_k \omega_k \{\alpha_k^\dagger \alpha_k + \beta_k^\dagger \beta_k\}\right), \tag{6}$$

where the sum is performed over half of the first Brillouin zone, and the operators α_k and β_k are introduced by the Bogoliubov transformation,

$$\begin{aligned} \alpha_k &= \cosh\theta_k\, a_k - \sinh\theta_k\, b_{-k}^\dagger, \\ \beta_k^\dagger &= \cosh\theta_k\, b_{-k}^\dagger - \sinh\theta_k a_k. \end{aligned} \tag{7}$$

In (7), a_k and $b_{-k}^\dagger$ are the Fourier transforms of the original boson operators,

$$\begin{aligned} a_k &= \frac{1}{\sqrt{N}}\sum_l a_{2l} e^{ik(2l-1/2)}, \\ b_{-k}^\dagger &= \frac{1}{\sqrt{N}}\sum_l b_{2l+1}^\dagger e^{-ik(2l+1/2)}, \end{aligned} \tag{8}$$

where the lattice constant was set equal to unity.

The energy $\varepsilon = \langle H\rangle$ and the dispersion relation ω_k are obtained after minimizing the free energy under the constraint of zero site magnetization, that is, $\langle T_{2l}^z\rangle = \langle S_{2l+1}^z\rangle = 0$. In this way, we obtain

$$\mathcal{E} = -2NJ_1\{[S - (f(0) - \tfrac{1}{2} - g(\boldsymbol{\delta}))]^2 - j[S - (f(0) - \tfrac{1}{2} - f(2\boldsymbol{\delta}))]^2\}, \tag{9}$$

where δ is a vector between nn sites, and we have used the definitions

$$\begin{aligned} f(r_{2l} - r_{2l'}) = f(r_{2l+1} - r_{2l'+1}) &= \frac{1}{2N}\sum_k e^{ik(2l-2l')}\phi_k \cosh 2\theta_k, \\ g(r_{2l} - r_{2l'+1}) &= \frac{1}{2N}\sum_k e^{ik(2l-2l'-1)}\phi_k \sinh 2\theta_k, \end{aligned} \tag{10}$$

where $\phi_k = 2n_k + 1$, n_k is the usual occupation number, $n_k = \langle\alpha_k^\dagger\alpha_k\rangle = \langle\beta_k^\dagger\beta_k\rangle = [\exp(\omega_k/T) - 1]^{-1}$, and θ_k is given by

$$\tanh 2\theta_k = \frac{\eta\cos k}{1 - \Gamma\sin^2 k}. \tag{11}$$

In the MSW theory, the expression for the dispersion relation is

$$\omega_k = \lambda\sqrt{(1 - \Gamma\sin^2 k)^2 - \eta^2\cos^2 k}. \tag{12}$$

In (12), we have introduced the parameters λ, μ, η, and Γ, which are defined by the relations

$$\lambda = 2J_1 g(\boldsymbol{\delta}) - \mu, \tag{13}$$

$$\eta = \frac{2J_1 g(\boldsymbol{\delta})}{\lambda}, \tag{14}$$

$$\Gamma = \frac{4jJ_1 f(2\boldsymbol{\delta})}{\lambda}. \tag{15}$$

In the equations above, μ is the Lagrange multiplier used in the minimization of the free energy under the restriction of zero site magnetization, and Γ is the parameter related to the inclusion of the nnn interactions.

The quantities of our interest, that is, the ground-state energy, the dispersion relation, the gap, defined here as $\omega_{k=0}$, and the spin–spin correlation function, can be obtained after the parameters defined in (13)–(15) are known. These parameters are obtained after solving the following set of self-consistent equations:

$$\begin{aligned} 2S+1 &= \frac{\lambda}{N}\sum_k \frac{1-\Gamma\sin^2 k}{\omega_k}\coth\left(\frac{\omega_k}{2T}\right), \\ \frac{\eta\lambda}{2J_1} &= \frac{\lambda}{2N}\sum_k \frac{\eta\cos^2 k}{\omega_k}\coth\left(\frac{\omega_k}{2T}\right), \\ \frac{\Gamma\lambda}{4J_1} &= \frac{\lambda j}{2N}\sum_k \frac{\cos(2k)(1-\Gamma\sin^2 k)}{\omega_k}\coth\left(\frac{\omega_k}{2T}\right). \end{aligned} \tag{16}$$

These equations were solved for $0 \leqslant j \leqslant j_{\max} = 0.30$. We cannot find solutions to the set of self-consistent equations for $j > j_{\max}$ because the MSW procedure considered here departs from the boson transformation defined in (2) which accounts only for small deviations from the Néel order. According to the classical spin-wave theory, the ground state is Néel-like for $j = 0$. The nnn interaction introduces frustration into the system and the Néel state cannot be the true ground state for large values of j where we expect that each sublattice has some kind of spiral alignment. Therefore, for large j, the ground state may be obtained from the Néel state by applying a uniform twist along the chain direction. In the $S \to \infty$ limit, a classical treatment shows that the ground state is in the Néel phase for $j < 0.25$, and in a spiral phase for $j > 0.25$. In their work, Kolezhuk *et al* [8] found a disorder point at $j_{\mathrm{D}} = 0.284(1)$ marking the onset of incommensurate spin–spin correlations in the chain. This disorder point is related to the existence of two low-temperature phases, the Néel and spiral phases. There is also a Lifshitz point at $j_{\mathrm{L}} = 0.3725$ [8], identified by the appearance of a two-peaked structure function for $j > j_{\mathrm{L}}$. Tonegawa *et al* [7] also restricted their numerical calculation to the $0 < j < 0.40$ region because they identified an incommensurate character for larger j. Therefore, we suggest that the lack of a numerical solution to the set of self-consistent equations (16) for $j > j_{\max}$ is related to this change in the ground state.

The ground-state energy can be obtained from (9), using $S = 1$, and our result is shown in figure 1 (circles), where we also represent the numerical estimates obtained by Tonegawa *et al* [7] (squares) using an exact diagonalization method. As can be seen in that figure, our results are in very good agreement with the numerical ones.

In the range investigated, we obtain $\eta < 1$ for any temperature, implying that there is a non-zero gap for the frustrated antiferromagnetic model, $S = 1$, as predicted by theoretical studies [9, 10] and more sophisticated numerical techniques [7, 8, 30]. The gap at zero temperature, Δ_0, as a function of the frustration parameter is shown in figure 2. We can see that the competition between the antiferromagnetic nn and nnn interactions stabilizes the gap since Δ_0 increases with j. The gap at zero temperature as a function of j was also obtained by Pati *et al* [30] and Kolezhuk *et al* [8] by using the density matrix renormalization group (DMRG) method. Their results show that Δ_0 increases with j for $j < 0.4$; for larger j, the gap decreases up to $j \approx 0.74$, where a topological phase transition occurs [13]. However, the magnitude of the gap determined in our procedure is much smaller (by a factor of 5) than the gap determined by the DMRG method. This kind of numerical discrepancy between numerical and analytical estimates for the gap has also been observed for the non-frustrated antiferromagnetic Heisenberg model (the Haldane system) not only for estimates obtained by using the MSW

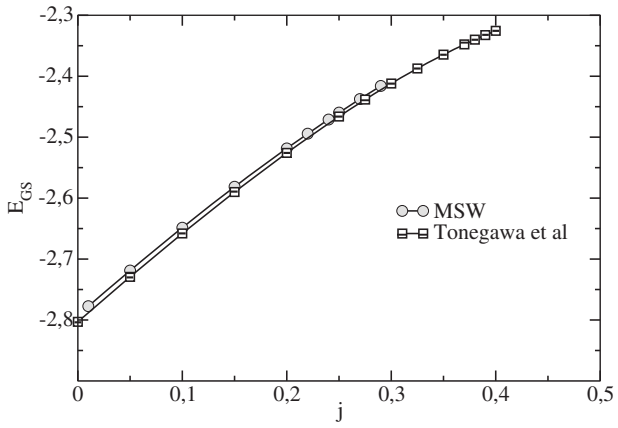

Figure 1. Ground-state energy, E_{GS}, as a function of j for $S = 1$. The MSW results (circles) are compared to numerical data [7] (squares) available in the literature.

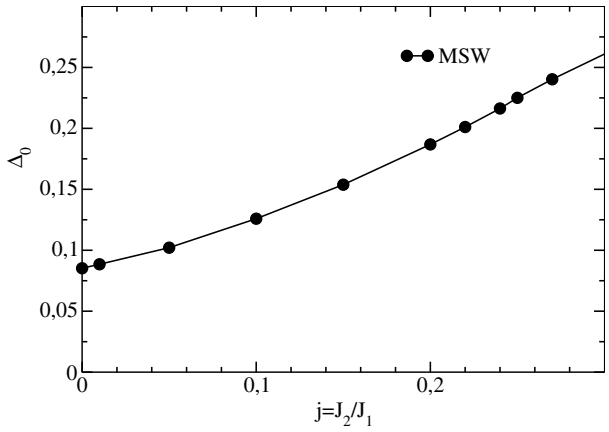

Figure 2. Gap at zero temperature, Δ_0, as a function of j obtained from the MSW approach, for $S = 1$.

theory but also from calculations based in the nonlinear σ model [32]. In fact, up to the present moment, no analytical approach is able to predict the correct magnitude of Δ_0 as a function of microscopic parameters. Therefore, in order to compare our results to the numerical ones obtained by Tonegawa *et al* [7] and Pati *et al* [30], we compare the normalized gap, that is, the gap obtained for a given j at zero temperature, $\Delta(T = 0)$, divided by the gap for $j = 0$, at $T = 0$, as a function of j. This result is displayed in figure 3, where we see that the MSW results predict the ratio $\Delta(T = 0)/\Delta_0$ to increase with j more quickly than the numerical results. Figure 4 shows the behaviour of the normalized gap, for $j = 0.00, 0.05, 0.10$ and 0.20, as a function of the normalized temperature: the gap increases with temperature in essentially the same way for all j shown.

The spin–spin correlation as a function of r, the distance between spins, is shown in figure 5. As could be expected, the correlation function, $\langle \mathbf{S}_i \cdot \mathbf{S}_j \rangle$, decays more quickly with r as j increases. The asymptotic behaviour of $\langle \mathbf{S}_i \cdot \mathbf{S}_j \rangle$ can be nicely fitted by the function $\exp(-r/\xi)/\sqrt{r}$, where ξ is identified as the correlation length: our results show that ξ decreases

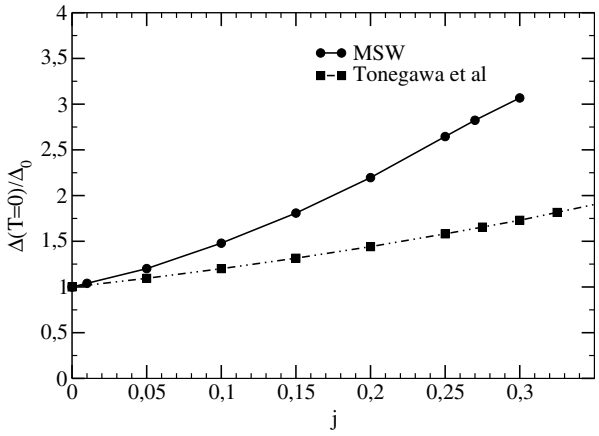

Figure 3. Gap at zero temperature, $\Delta(T = 0)$, normalized by the gap at zero temperature for $j = 0$, Δ_0, as a function of j for $S = 1$. The MSW results (full circles) are compared to the numerical results obtained by Tonegawa *et al* [7] (full squares).

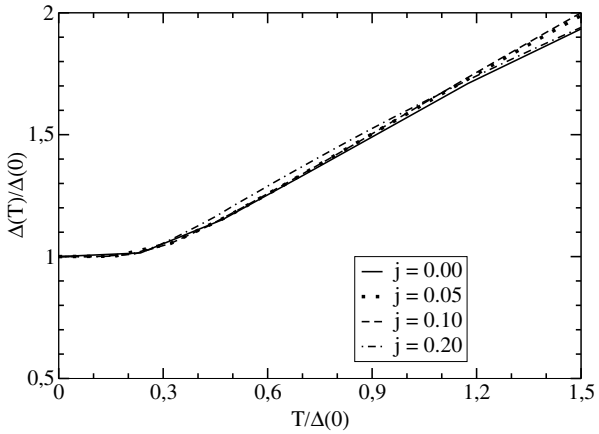

Figure 4. Gap at temperature T, $\Delta(T)$, normalized by the value of the gap at zero temperature for each j value, $\Delta(0)$, as a function of the normalized temperature, $T/\Delta(0)$, for $j = 0.00, 0.05, 0.10$, and 0.20 for $S = 1$.

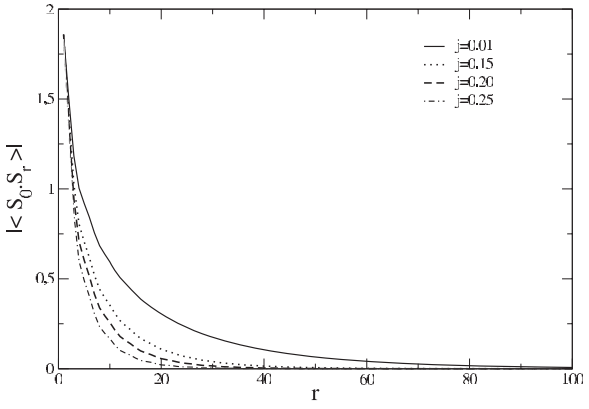

Figure 5. Correlation function $|\langle \mathbf{S}_0 \cdot \mathbf{S}_r \rangle|$, as a function of the distance r, for several values of j.

as j increases. Figure 6 shows the point, r_f, at which our numerical results start to agree with the asymptotic expansion, as a function of the frustration parameter.

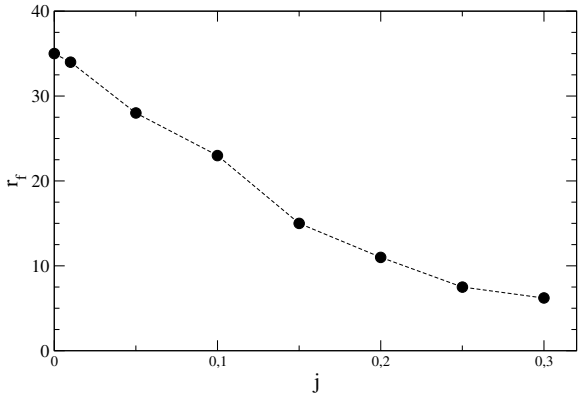

Figure 6. The point, r_f, at which our numerical results start to agree with the asymptotic expansion, as a function of the frustration parameter.

3. The projection operator method and results

The method adopted here for the calculation of the dynamic correlation function—a projection operator method including up to two magnon processes—is valid in the low-temperature range. We notice that, to our knowledge, this is the first attempt to obtain the dynamical behaviour of Hamiltonian (1).

We must also remark that a first attempt to study the dynamic properties of (1) could be done, with greater simplicity, in the spin-wave framework by calculating quantities like $\langle S_i(t)S_j(0)\rangle$ and its transforms: such a procedure was applied by many other authors to get information about the dynamical behaviour of other spin systems. Despite its simplicity, this last procedure—which will be referred to here as 'the usual spin-wave dynamic method'—has some drawbacks when compared to the method adopted in this work. For example, magnon scatterings are not included in the simpler procedure and, therefore, our calculation is, in this sense, more advanced. An interesting discussion concerning the similarities and differences between the usual spin-wave dynamic method and the projection operator method can be found in [33] and [34], which compare the results obtained by applying each of these two methods to 1D and 2D Heisenberg ferromagnets.

In antiferromagnets, spin waves have two flavours, one associated with the conventional magnetization, $M_q^\alpha = S_q^\alpha + T_q^\alpha$, and the other with the staggered magnetization, $\mathcal{R}_q^\alpha = S_q^\alpha - T_q^\alpha$, with $\alpha = x, y, z$. At low temperatures, the $\mathcal{R}_q^\alpha$ correlation function is the leading contribution to the structure factor near the antiferromagnetic wavevector [28, 19] and, in this work, we will be concerned with its calculation. The calculation of the M_q^α function could also be done in the same framework but this will not be our task in this work.

We emphasize that only rotationally invariant quantities such as $\mathcal{R}_q = \frac{1}{3}(\mathcal{R}_q^x + \mathcal{R}_q^y + \mathcal{R}_q^z)$ are calculated here. Due to the isotropic character of Hamiltonian (1), each of the three spin components gives the same contribution to the dynamical behaviour of the model. However, the Dyson–Maleev transformation breaks the symmetry of the spin space, giving a privileged rule to the z-component. Therefore, we restore the model's symmetry by computing rotationally invariant quantities.

In the following, we describe the main steps leading to the calculation of the dynamic correlation function. A detailed description of the procedure can be found in [15, 16]. One of the advantages of this procedure is that it allows us to obtain the structure factor for all values of

the wavevector q, while calculations based on the nonlinear σ model are restricted to the long-wavelength limit $q \to 0$. The Fourier transform of the relaxation function is given by [35]

$$R(q,\omega) = \frac{1}{2\pi}\int_{-\infty}^{\infty} \mathrm{d}t\, \mathrm{e}^{-\mathrm{i}\omega t}\frac{(\mathcal{R}_q(t),\mathcal{R}_q(0))}{(\mathcal{R}_q,\mathcal{R}_q)}. \tag{17}$$

Here, (A, B) is the Kubo inner product of two operators A and B, defined as [36]

$$(A,B) = \frac{1}{\beta}\int_0^{\beta} \langle \mathrm{e}^{\lambda H} A^{\dagger} \mathrm{e}^{-\lambda H} B\rangle \,\mathrm{d}\lambda, \tag{18}$$

where $\langle\cdots\rangle$ denotes the usual thermal average and $\beta = 1/k_{\mathrm{B}}T$. One can show that, after some analytical work, the dynamical correlation function $R(q,\omega)$ is given by

$$R(q,\omega) = \frac{(\mathcal{R}_q,\mathcal{R}_q)\langle\omega_q^2\rangle\Sigma_q''(\omega)}{[\omega^2 - \langle\omega_q^2\rangle + \omega\Sigma_q'(\omega)]^2 + [\omega\Sigma_q''(\omega)]^2}, \tag{19}$$

where $\Sigma_q'(\omega)$ and $\Sigma_q''(\omega)$ are the real and imaginary parts of the second-order memory function $\Sigma_q(\omega)$, respectively. In time space, this memory function is expressed by

$$\Sigma_q(t) = -\frac{(QL^2\mathcal{R}_q, \mathrm{e}^{-\mathrm{i}QLQt}QL^2\mathcal{R}_q)}{(L\mathcal{R}_q, L\mathcal{R}_q)}, \tag{20}$$

where Q is a projection operator that projects out any term proportional to $\mathcal{R}_q$ and $L\mathcal{R}_q$, with L being the Liouville operator defined by the relation $LA = -\mathrm{i}[A, H]$. Reiter [15] has shown that, to leading order in temperature, the operator Q in the exponential function (20) can be dropped, so we can write

$$QL^2\mathcal{R}_q = L^2\mathcal{R}_q - \langle\omega_q^2\rangle\mathcal{R}_q. \tag{21}$$

In equation (19), we also need to calculate the second frequency moment $\langle\omega_q^2\rangle$, given by

$$\langle\omega_q^2\rangle = \frac{(L\mathcal{R}_q, L\mathcal{R}_q)}{(\mathcal{R}_q,\mathcal{R}_q)}. \tag{22}$$

The second time derivative needed to evaluate the numerator of the memory function (20) is directly obtained from the definition of the Liouville operator and from (1). The whole calculation is very straightforward but the expressions are enormous, and, for brevity, we will not show them here. The next step requires us to apply the Dyson–Malleev (2) and Bogoliubov (7) transformations for the spin operators in those expressions—as done in the previous section. As shown by Reiter [15], we can, to leading order in temperature, replace the time evolution $\exp(-\mathrm{i}LT)$ by the harmonic time evolution, that is

$$\begin{aligned} \alpha_q(t) &= \mathrm{e}^{-\mathrm{i}\omega_q t}\alpha_q(0), \\ \alpha_q^{\dagger}(t) &= \mathrm{e}^{\mathrm{i}\omega_q t}\alpha_q^{\dagger}(0), \end{aligned} \tag{23}$$

and similar equations for $\beta_q(t)$ and $\beta_q^{\dagger}(t)$. So, we are left with a number of Kubo products of four bosonic operators which can be decoupled by using standard procedures. After a tedious but simple calculation, we get

$$\Sigma_q(t) = \frac{2}{N}\sum_k [\mathcal{A}_-(q,k)\cos(\Omega_- t) + \mathcal{A}_+(q,k)\cos(\Omega_+ t)], \tag{24}$$

where $\mathcal{A}_-$ and $\mathcal{A}_+$ are given by

$$\begin{aligned} \mathcal{A}_-(q,k) &= \frac{[\Gamma_1(q,k)]^2}{(L\mathcal{R}_q, L\mathcal{R}_q)} \times \frac{(\mathrm{e}^{\beta\omega_k} - \mathrm{e}^{\beta\omega_{q-k}})}{\beta\Omega_-} n_k n_{q-k}, \\ \mathcal{A}_+(q,k) &= \frac{[\Gamma_2(q,k)]^2}{(L\mathcal{R}_q, L\mathcal{R}_q)} \times \frac{(\mathrm{e}^{\beta\Omega_+} - 1)}{\beta\Omega_+} n_k n_{q-k}. \end{aligned} \tag{25}$$

In the definitions of $\mathcal{A}_\pm$ we have used

$$\begin{aligned}\Gamma_1(q,k) &= D_1(q,k)[u_k v_{q-k} + u_{q-k} v_k] - D_2(q,k)[u_k u_{q-k} + v_{q-k} v_k],\\ \Gamma_2(q,k) &= D_1(q,k)[u_k u_{q-k} + v_{q-k} v_k] - D_2(q,k)[u_k v_{q-k} + u_{q-k} v_k],\end{aligned} \tag{26}$$

where

$$\begin{aligned}D_1(q,k) &= 8J_1^2S^2\{\cos(k)[1-2j\sin^2(q-k)] + \cos(q-k)[1-2j\sin^2(k)]\},\\ D_2(q,k) &= 4J_1^2S^2\{[\cos(k)+\cos(q-k)]^2 + 2j^2[\cos(2k)\\ &\quad - \cos(2q-2k)] \times [\sin^2(k) - \sin^2(q-k)]\} + \langle\omega_q^2\rangle.\end{aligned}$$

In the expressions above, n_q is, as before, the boson occupation number and $\Omega_\pm$ is defined as

$$\Omega_\pm = \omega_k \pm \omega_{q-k}. \tag{27}$$

The expression for $(L\mathcal{R}_q, L\mathcal{R}_q)$ is also needed for evaluation of the second moment which, according to (22), is given by the ratio of the two expressions below:

$$(L\mathcal{R}_q, L\mathcal{R}_q) = \frac{8(J_1S)^2}{N}\sum_k \left\{F_1^2(q,k)\frac{(\mathrm{e}^{\beta\omega_k} - \mathrm{e}^{\beta\omega_{q-k}})}{\beta\Omega_-} + F_2^2(q,k)\frac{(\mathrm{e}^{\beta\Omega_+}-1)}{\beta\Omega_+}\right\} n_k n_{q-k} \tag{28}$$

and

$$\begin{aligned}(\mathcal{R}q, \mathcal{R}_q) = \frac{2}{N}\sum_k \Bigg\{&\frac{(\mathrm{e}^{\beta\omega_k} - \mathrm{e}^{\beta\omega_{q-k}})}{\beta\Omega_-}[u_k u_{q-k} + v_k v_{q-k}]^2\\ &+ \frac{(\mathrm{e}^{\beta\Omega_+}-1)}{\beta\Omega_+}[u_k v_{q-k} + u_{q-k} v_k]^2\Bigg\} n_k n_{q-k}.\end{aligned} \tag{29}$$

In (28), we have used

$$\begin{aligned}F_1(q,k) &= [\cos(k)+\cos(q-k)][u_k v_{q-k} - u_{q-k} v_k]\\ &\quad + j[\cos(2k) - \cos(2q-2k)][u_k u_{q-k} - v_k v_{q-k}],\\ F_2(q,k) &= [\cos(k)+\cos(q-k)][u_k u_{q-k} - v_k v_{q-k}]\\ &\quad + j[\cos(2k) - \cos(2q-2k)][u_k v_{q-k} - u_{q-k} v_k].\end{aligned}$$

Taking the Laplace transform of the memory function (24) and, then, applying the Cauchy formula we finally obtain the expressions for the real and imaginary parts of the memory function as given by

$$\Sigma_q'(\omega) = \frac{1}{2\pi^2}\mathcal{P}\int\left\{\frac{\mathcal{A}_-(q,k)}{\omega+\Omega_-} + \frac{\mathcal{A}_-(q,k)}{\omega-\Omega_-} + \frac{\mathcal{A}_+(q,k)}{\omega+\Omega_+} + \frac{\mathcal{A}_+(q,k)}{\omega-\Omega_+}\right\}, \tag{30}$$

and

$$\begin{aligned}\Sigma_q''(\omega) = \frac{1}{2\pi}\sum_{k_i}\Bigg\{&\frac{\mathcal{A}_-(q,k)}{|\mathrm{d}\Omega_-/\mathrm{d}k|_{k_1}}[\delta(\omega+\Omega_-) + \delta(\omega-\Omega_-)]\\ &+ \frac{\mathcal{A}_+(q,k)}{|\mathrm{d}\Omega_+/\mathrm{d}k|_{k_2}}[\delta(\omega+\Omega_+) + \delta(\omega-\Omega_+)]\Bigg\},\end{aligned} \tag{31}$$

where the k_i with $i = 1, 2$ correspond to the roots of $\omega = |\Omega_-(q,k_1)|$ and $\omega = |\Omega_+(q,k_2)|$, and the summation is performed over half of the first Brillouin zone.

The method employed here is restricted to the low-temperature regime, that is, $T \ll J$, but, as discussed by Reiter [15], it is exact to leading order in temperature. The extension of the wavevector region depends on how precise are the expressions to be used for the static quantities required by the memory function formalism. If we had exact expressions for, say, the

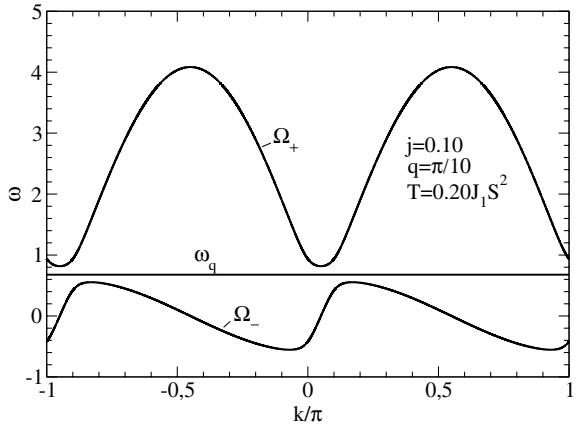

Figure 7. Ω_- e Ω_+ as a function of k/π for $j = 0.10$, $q = \pi/10$ and $T = 0.20J_1S^2$. The horizontal line corresponds to the spin-wave energy ω_q.

second moment, the whole wavevector range would be covered by this technique. However, as the second moment is calculated in the context of the MSW theory, we are bound to the same domain of that theory, that is, $q > \xi^{-1}$, where ξ is the correlation length. In the following paragraphs, we discuss our numerical results for the dynamic correlation function calculated from the above expressions.

Several features of the dynamic correlation function can be understood by analysing the Ω_+ and Ω_- functions due to the relationship between these two functions and the real and imaginary parts of the memory function, given by equations (30) and (31). The $\Omega_\pm$ functions for $j = 0.10$, $q = \pi/10$, and $T = 0.20J_1S^2$ are plotted in figure 7. The horizontal line in figure 7 represents the spin-wave energy for the chosen parameters. An examination of equation (31) leads us to expect divergences at the maxima and minima of $\Omega_\pm$, that is, at the wavevectors where the two-magnon density of states

$$n_\pm = \left| \frac{\mathrm{d}k}{\mathrm{d}\Omega_\pm(q,k)} \right| \tag{32}$$

diverges. From figure 7, we expect Σ'' to diverge at three frequencies: $\omega = \Omega_1$, the absolute value of the Ω_- maximum and minimum, $\omega = \Omega_2$, the minimum, and $\omega = \Omega_3$, the maximum of Ω_+. In that figure, the behaviour of $\Omega_\pm$ as a function of k/π for $T = 0.2J_1S^2$ can be compared to the one obtained for the non-frustrated case [28]: the main difference is that for the frustrated case ($j = 0.1$) the frequency difference, $\Delta\omega = \Omega_2 - \Omega_1$, is larger (0.26) than the one found in the non-frustrated case (0.20) [28]. As we will discuss below, this difference is intimately related to the zero energy gap, which, as shown in the previous section, increases with j.

The Ω_+ and Ω_- curves never cross, and therefore, due to the delta functions in (31), the damping will either receive contributions from Ω_- for $\omega \leqslant |\Omega_1|$, or from Ω_+ in the frequency region $\Omega_2 \leqslant \omega \leqslant \Omega_3$. The contributions from Ω_- correspond to the absorption and reemission of a magnon, called a difference process, while the contributions from Ω_+ correspond to the creation of two magnons, a sum process. We thus conclude that for $\Omega_1 < \omega < \Omega_2$, none of these two processes can contribute to the damping, that is, $\Sigma''(q,\omega) = 0$, and, consequently, $R(q,\omega) = 0$, in a frequency range equal to $\Delta\omega$, approximately centred at the spin-wave energy ω_q. This feature is a consequence of the existence of a gap in the spin-wave dispersion relation ($\Delta\omega \propto \omega_{q=0}$) and will be present in any theory that includes only two-magnon processes.

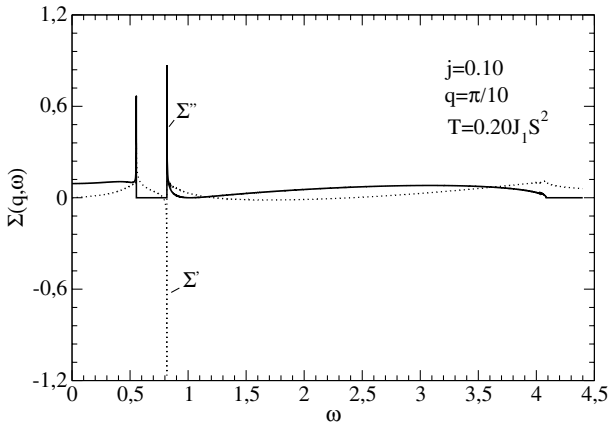

Figure 8. Σ''_q (continuous line) and Σ'_q (dashed line) as a function of ω for $j = 0.10$, $q = \pi/10$ and $T = 0.20J_1S^2$.

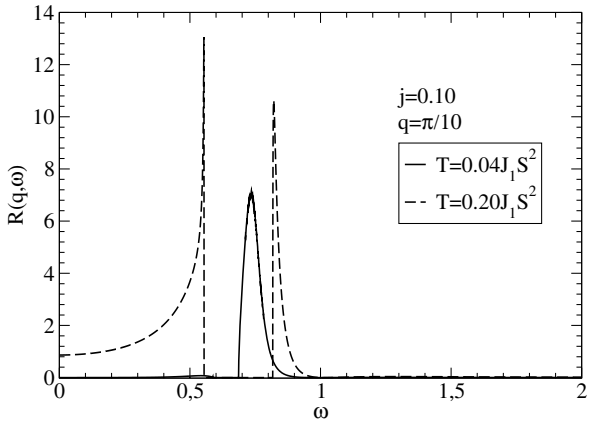

Figure 9. $R(q, \omega)$ as a function of ω for $j = 0.10$, $q = \pi/10$ and $T = 0.04J_1S^2$ (continuous line) and $T = 0.20J_1S^2$ (dashed line).

The real and imaginary parts of the memory function for $j = 0.10$, $q = \pi/10$, and $T = 0.20J_1S^2$ are shown in figure 8. The dynamic correlation function, $R(q, \omega)$, for the same parameters, and also for $T = 0.04J_1S^2$, is shown in figure 9. In figure 8, we see that Σ'' is not as sharply peaked at Ω_3 as it is at Ω_1 and Ω_2. Obviously, in a numerical calculation, the divergences of (31) will only be met if one points exactly at the precise value of the wavevector satisfying $d\Omega_\pm/dk = 0$. Then, we will not get a really divergent result for Σ'': the values obtained depend on the values (small) of the derivatives $(d\Omega_\pm/dk)$ in the neighbourhood of the critical point and, also, on the numerator, $\mathcal{A}_\pm$, given by equations (25). The functions $\mathcal{A}_\pm$ depend on the occupation numbers which are small at high temperatures ($T = 0.2J_1S^2$) and high frequencies: for this reason, in Σ'' (figure 8), the effect of the divergence at Ω_3 is not so sharp as the ones at Ω_1 and Ω_2.

For larger wavevectors, such as, for example, $q = \pi/4$, we find that Ω_+ has an absolute maximum (Ω_3) and a local maximum at a frequency value close to Ω_2. This means that we expect a peaked behaviour for Σ'' at a fourth frequency: the one corresponding to the local maximum in Ω_+. The effect of this fourth frequency can be seen in figure 10, where we show $R(q, \omega)$ for $q = \pi/4$, $j = 0.10$ and two temperatures $T/J_1S^2 = 0.04$ and 0.12: comparing with the result shown in figure 9, we see that the contribution due to the sum process has a richer structure in figure 10. In the following, we will discuss our results for $R(q, \omega)$ for a small wavevector, $q = \pi/10$, and for a moderately large wavevector, $q = \pi/4$.

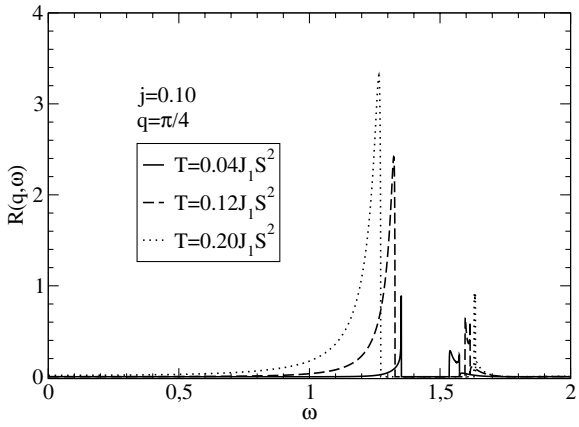

Figure 10. $R(q, \omega)$ as a function of ω for $j = 0.10$, $q = \pi/4$ for three values of T.

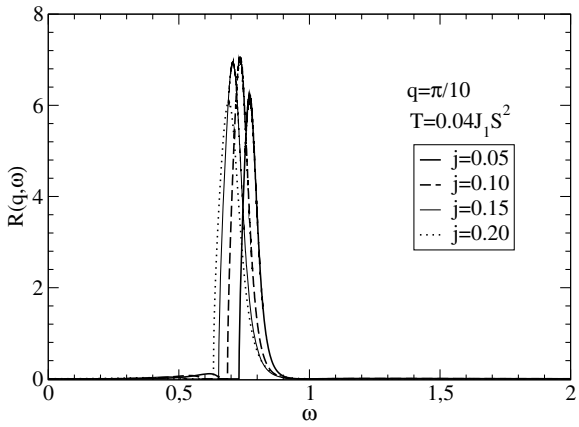

Figure 11. $R(q, \omega)$ as a function of ω for $q = \pi/10$, $T = 0.04 J_1 S^2$ for several values of j.

For $q = \pi/10$, $j = 0.10$, and low temperature ($T/J_1S^2 = 0.04$), the dynamic correlation function exhibits a single peak, as can be seen in figure 9: this peak corresponds to the contribution from Ω_+. As the temperature is raised (figure 9 for $T/J_1S^2 = 0.20$), the number of magnons in the system increases and the peak related to Ω_- appears. The frequency region, $\Delta\omega$, where $R(q, \omega)$ is null becomes wider with temperature increases and the distance between the two peaks gets bigger: for $T/J_1S^2 = 0.20$ the two peaks are well defined and separated.

A typical behaviour for $R(q, \omega)$ in the large-wavevector region is displayed in figure 10, where we plot the dynamic correlation function for $q = \pi/4$, $j = 0.10$, $T/J_1S^2 = 0.04$, 0.12, and 0.20. Notice that, in the temperature range shown, there is basically a single peak which is due to the contribution from Ω_-, or better, to the absorption and reemission of a magnon. The peak due to the contribution from Ω_+ has small intensity and is too narrow (it becomes narrower as T increases) to be experimentally observable. The explanation for this behaviour is that magnons with large wavevectors require a large amount of energy to be created and, then, difference processes have a higher probability of occurring.

We now discuss the effect of enhancing the frustration in the system. The effect of the frustration parameter, at $T/J_1S^2 = 0.04$ and 0.20, for $q = \pi/10$ and $q = \pi/4$, is shown in figures 11–14 for $j = 0.05, 0.10, 0.15$, and 0.20. A common feature in those figures is that the increment on j makes the parameter Γ larger and, therefore, the spin-wave energy, equation (12), for a specific wavevector decreases. This explains why the peaks related to

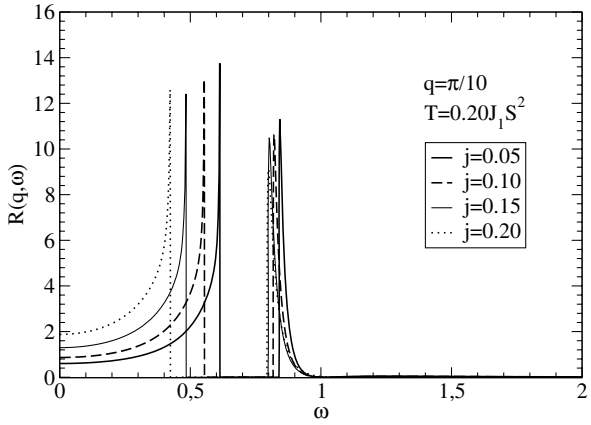

Figure 12. $R(q, \omega)$ as a function of ω for $q = \pi/10$, $T = 0.20 J_1 S^2$ for several values of j.

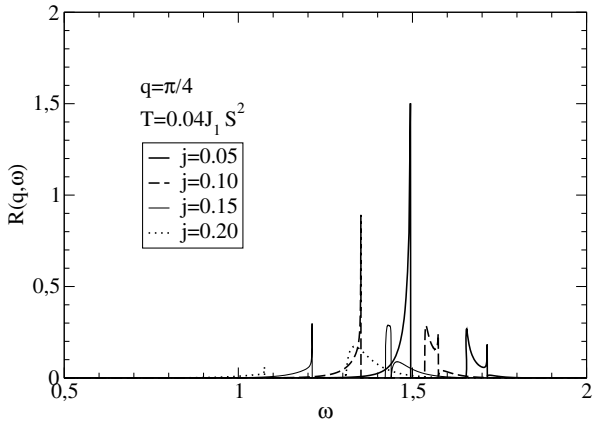

Figure 13. $R(q, \omega)$ as a function of ω for $q = \pi/4$, $T = 0.04 J_1 S^2$ for several values of j.

contributions from the Ω_+ and Ω_- functions move to lower frequencies as j increases. Also, as j increases, the gap energy and, therefore, $\Delta\omega$, become larger, and so does the distance between the two peaks in $R(q, \omega)$.

For the smaller wavevector, $q = \pi/10$, for all j and temperatures shown in figures 11 and 12, we observe no other changes due to the variation of j: for $T/J_1 S^2 = 0.04$, there is basically a single peak—the one related to Ω_+—whose intensity does not vary appreciably. For higher temperature, $T/J_1 S^2 = 0.20$, the peak related to the difference process develops and, as j increases, the intensity at low frequencies ($\omega \to 0$) becomes higher; however, roughly speaking, we may say that the areas under each of the two peaks do not suffer sharp variations. We then conclude that, for small wavevectors, we have a single peak at low temperatures and a double peak for higher temperature: as T and j increase, the distance between the two peaks becomes bigger.

An examination of figure 13, for $q = \pi/4$ and $T/J_1 S^2 = 0.04$, shows that the main peak in $R(q, \omega)$ (the one related to Ω_-) is quite small and decreases appreciably as j increases: this suggests that, for low temperatures, magnons with such high wavevectors have a small chance to be found in the system and the contribution from two-magnon processes to the

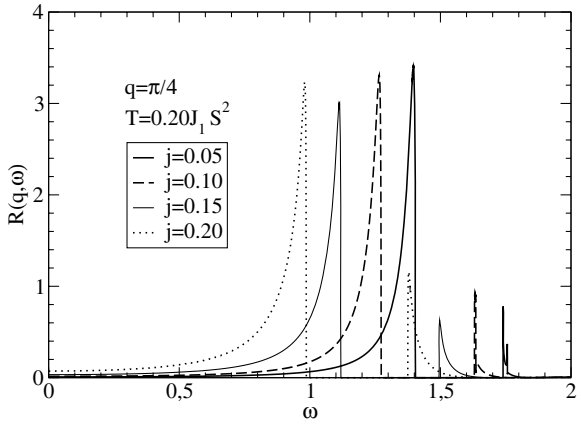

Figure 14. $R(q, \omega)$ as a function of ω for $q = \pi/4$, $T = 0.20 J_1 S^2$ for several values of j.

dynamic correlation function is very small. As could be expected, for higher temperature, $T/J_1S^2 = 0.20$, even energetic magnons can be created, and the peak in $R(q, \omega)$ for $q = \pi/4$ becomes significant.

4. Conclusion

In this paper, we have investigated static and dynamic properties of the frustrated antiferromagnetic Heisenberg chain by combining the MSW theory to the memory function formalism. The MSW theory was used to obtain static quantities [31] such as the ground-state energy, the dependence of the gap with the temperature and the frustration parameter, the spin-wave dispersion relation and the behaviour of the spin–spin correlation function. The MSW results for the ground-state energy are in good agreement with numerical data available in the literature [7]. Although the MSW estimates for the gap, as a function of the frustration parameter and the temperature, are much smaller than the ones obtained by more sophisticated numerical techniques [7, 8, 30], we obtain a qualitative agreement leading to an increasing of the gap as j and T increases. The asymptotic behaviour of the spin–spin correlation function decays with the distance r as $\exp(-r/\xi)/\sqrt{r}$, and, as could be expected, the correlation length ξ decreases as j increases.

The dynamical correlation function was obtained for several j values, for low ($T/J_1S^2 = 0.04$) and moderately high (0.20) temperatures: we showed that there are two distinct behaviours concerning the dependence on the wavevector. For small q and low temperature, $R(q, \omega)$ shows a single peak corresponding to the process of two-magnon creation: as the temperature is raised, a second peak, the one related to contributions from absorption and reemission of a magnon, develops. This second peak is well split from the first one and it is difficult to suppose that the inclusion of higher-order processes (such as, for example, three-magnon scattering) in the calculation of $R(q, \omega)$ will fill up the region separating them.

For larger wavevectors, the contribution from Ω_- is always dominant. However, if the temperature is not high enough to allow the presence of high-energy magnons, the contribution to $R(q, \omega)$ can be negligible. Therefore, for large q, we expect a single peak only for moderately high temperature.

The analytical procedure adopted in this work to calculate the dynamical correlation function has been proved [15, 16, 28, 18, 19] to be successful in the low-temperature region.

Therefore, as we have presented here the first attempt to obtain the dynamical behaviour of the frustrated antiferromagnetic Heisenberg chain, we hope that our results will stimulate further numerical and experimental investigations concerning the dynamic behaviour of the model. The $\Delta\omega$ region around the spin-wave energy, giving a null result for the dynamical correlation in this region, is not, as could be thought, a spurious result of the method: this feature will be shared by any theory including only two-magnon processes.

References

[1] Haldane F D M 1983 *Phys. Lett.* A **93** 464
Haldane F D M 1983 *Phys. Rev. Lett.* **50** 1153
[2] White S R and Affleck I 1996 *Phys. Rev.* B **54** 9862
[3] Majumdar C K 1970 *J. Phys. C: Solid State Phys.* **3** 911
[4] Shastry B S and Sutherland B 1981 *Phys. Rev. Lett.* **47** 964
[5] Nomura K and Okamoto K 1994 *J. Phys. A: Math. Gen.* **27** 5773
Nomura K and Okamoto K 1993 *J. Phys. Soc. Japan* **62** 1123
[6] Okamoto K and Nomura K 1992 *Phys. Lett.* A **169** 433
[7] Tonegawa T, Kaburagi M, Ichikawa N and Harada I 1992 *J. Phys. Soc. Japan* **61** 2890
[8] Kolezhuk A K, Roth R and Shollwöck U 1996 *Phys. Rev. Lett.* **77** 5142
Kolezhuk A K, Roth R and Shollwöck U 1997 *Phys. Rev.* B **55** 8928
[9] Rao S and Sen D 1994 *Nucl. Phys.* B **424** 547
[10] Allen D and Senechal D 1995 *Phys. Rev.* B **51** 6394
[11] Affleck I, Kennedy T, Lieb E H and Tasaki H 1987 *Phys. Rev. Lett.* **59** 799
Affleck I, Kennedy T, Lieb E H and Tasaki H 1988 *Commun. Math. Phys.* **115** 477
[12] den Nijs M and Rommelse K R 1989 *Phys. Rev.* B **40** 4709
Girvin S M and Arovas D P 1989 *Phys. Scr.* T **27** 156
Kennedy T and Tasaki H 1992 *Phys. Rev.* B **45** 304
[13] Kolezhuk A K and Schollwöck U 2002 *Phys. Rev.* B **65** 100401
[14] Hikihara T, Kaburagi M, Kawamura H and Tonegawa T 2000 *J. Phys. Soc. Japan* **69** 259
[15] Reiter G and Sjölander A 1977 *Phys. Rev. Lett.* **39** 1047
Reiter G 1980 *J. Phys. C: Solid State Phys.* **13** 3027
[16] De Raedt B, De Raedt H and Fivez J 1981 *J. Phys. Rev.* B **23** 4597
De Raedt B, De Raedt H and Fivez J 1981 *Phys. Rev. Lett.* **46** 3027
[17] Gouvêa M E and Pires A S T 1987 *J. Phys. C: Solid State Phys.* **20** 2431
[18] Menezes S L, Pires A S T and Gouvêa M E 1993 *Phys. Rev.* B **47** 12280
[19] Albuquerque A F, Pires A S T and Gouvêa M E 2005 *Phys. Rev.* B **72** 174423
[20] Pires A S T and Gouvêa M E 2004 *Braz. J. Phys.* **34** 1189
[21] Mermin N D and Wagner H 1966 *Phys. Rev. Lett.* **22** 1133
[22] Takahashi M 1987 *Phys. Rev. Lett.* **58** 168
[23] Hirsch J E and Tang S 1989 *Phys. Rev.* B **40** 4769
[24] Takahashi M 1989 *Phys. Rev.* B **40** 2494
[25] Okabe Y, Tikuchi M and Nagi D S 1988 *Phys. Rev.* B **61** 2971
[26] Chakravarty S, Halperin B I and Nelson D R 1989 *Phys. Rev.* B **39** 2344
[27] Xu J H and Ting C S 1990 *Phys. Rev.* B **42** 6861
[28] Pires A S T and Gouvêa M E 2002 *J. Magn. Magn. Mater.* **241** 315
[29] Sakaguchi T, Kakurai K, Yokoo T and Akimitsu J 1996 *J. Phys. Soc. Japan* **65** 3025
[30] Pati S, Chitra R, Sen S, Krishnamurthy H R and Ramasesha S 1996 *Europhys. Lett.* **33** 707
[31] Rocha-Filho G M, Pires A S T and Gouvêa M E 2007 *Eur. Phys. J.* B **56** 7
[32] Jolicoeur Th and Golinelli O 1994 *Phys. Rev.* B **50** 9265
[33] Reiter G 1993 *Phys. Rev.* B **47** 8335
[34] Takahashi M 1993 *Phys. Rev.* B **47** 8336
[35] Pires A S T 1988 *Helv. Phys. Acta* **61** 988
[36] Mori H 1965 *Prog. Theor. Phys.* **34** 399